International Journal of GEOMATE, April, 2025 Vol.28, Issue 128, pp.92-99
ISSN: 2186-2982 (P), 2186-2990 (O), Japan, DOI: https://doi.org/10.21660/2025.128.g14224
Geotechnique, Construction Materials and Environment

FLOOD AND INUNDATION RISK ANALYSIS DUE TO POTENTIAL LAND SUBSIDENCE ON ALLUVIAL PLAINS

Ade Tricia Miranda[1], *Dinar Dwi Anugerah Putranto[2] and Taufik Ari Gunawan[3]

[1]Doctoral Program in Engineering, Postgraduate Program, Faculty of Engineering, Sriwijaya University;
[2,3]Department of Civil Engineering and Planning, Faculty of Engineering, Sriwijaya University, Indonesia

*Corresponding Author, Received: 18 Jan. 2025, Revised: 25 Jan. 2025, Accepted: 07 Feb. 2025

ABSTRACT: Flood is capable of causing damage to residential areas, public facilities, and other infrastructure buildings. Areas with land use planning and land cover development that are not integrated are susceptible to experiencing flood and inundation problems. This is because regional development and spatial planning for public facilities do not consider the watershed storage capacity, leading to the inability to accommodate large amounts of runoff water. In Indonesia, the infrastructural and city development of Palembang requires extensive land reclamation because the area is an alluvial plain, characterized by swamp land. During land reclamation, storage capacity is considered, causing frequent floods and inundation in certain areas. Additionally, the phenomenon of land subsidence leads to rising river and sea water levels, which affects the low capacity of a watershed, making it no longer suitable. Based on the description, this research aimed to explore the watershed storage capacity to analyze flood problems occurring due to developments in land use and degradation through remote sensing image data. The analysis was carried out to evaluate changes in land cover (2014-2024) and the influence of land subsidence on reducing storage capacity in watershed areas to develop a flood control scenario. In this research, 2D modeling of flood events was performed to represent different land subsidence scenarios in 2014 and 2024. To determine flood area and variations in water depth, 2D HEC-RAS modeling was used to simulate flood inundation in the watershed area.

Keywords: Flood, Storage capacity, Land subsidence, Land use change

1. INTRODUCTION

Land deformation known as land subsidence is a geohazard caused by natural factors or human activities [1]. A factor that often occurs is the extraction of groundwater at a depth exceeding the permitted limit. Excessive water pumping in urban areas is caused by the need for clean water to meet the demand for services and trade by the population. Furthermore, high population growth in urban areas contributes to the increase in land for settlements and infrastructure [2], increased flooding[3,4], and inundation [5]. Other hazards include decreased capacity of the drainage system, which is no longer appropriate.

Many cities in the world face land subsidence cases, particularly in alluvial and delta plain areas such as Palembang [6]. In Indonesia, Palembang is among metropolitan cities with significant growth and development in the Musi River delta area, characterized by mostly alluvial soil structure [7]. However, the expansion of the city into Tanjung Api-api seaport is vulnerable to land subsidence, which can cause waterlogging or flooding due to river tides. Excessive land subsidence will endanger building structures, underground facilities, and human safety. One of the specific targets of the 9 evaluation indicators in accordance with the sub-goal of SDG (Sustainable Development Goals) 13.1 is "Strengthening and adapting capacity to threats and risks due to climate change". In relation to the SDG agenda, participation from the state is expected to consider risk reduction and prevention [8,9] and technology exploration [10].

The research on spatiotemporal land subsidence has shown that changes in land use due to direct human activities or basic material variables for reclamation affect the soil strength factor and cause alteration in the distribution [11,12]. Putranto et al, [13] stated that changes in land use in the urban fringe or upstream watershed significantly increased large runoff in the downstream urban areas. In Palembang City, Sarino found that the changes in land use contributed to 90.5% of the amount of run-off, caused by massive land subsidence. In a different area, Yustiana [14] analyzed the drainage channel in Rancaekek district, due to industrial development along the Cileunyi - Nagrek Highway route, which was always overpopulated by flood water.

Climate change has caused variations in rainfall patterns and intensity, leading to an increase in extreme flood events[15]. The development of settlements located along alluvial land is very vulnerable to land deformation, which causes an increase in flood inundation. Therefore, mitigation to reduce the socio-economic impacts of increased floods and inundation requires the development of control infrastructure by implementing better prediction methods [16]. With the development of technology, flood impact reduction strategies have

developed, starting from the hydraulic structure model to floodplain management and scenario analysis. Flood models using sophisticated software and remote sensing data have also facilitated tracking and reducing uncertainty in producing accurate flood risk maps, considering the impacts of climate change[17]. When the discharge in an open channel increases, the height of the water surface also rises along with a high volume of water. However, when the flood subsides, releasing the same volume of water from the reservoir prolongs the downstream flow and reduces the flood peak. The movement of waves in natural channels in their design and prediction is resolved by flood tracking. According to [18], flood tracking can be modeled and solved mathematically with hydrological and hydraulic equations.

Hydraulic models of river flow are widely used for flood simulation and management through hydraulic variables to design flood control scenarios [19]. 1D models are often used to efficiently simulate flow in channels. Meanwhile, 2D analysis in two dimensions allows visualization of flood extent, water depth, and flow velocity, requiring significant data to be analyzed digitally spatially[20]. According to Liu and Fang [21], 3D models consider three main components, namely flow velocity, 1D, and 2D modeling data, to improve the accuracy of the analysis results. The accuracy of the data source is very important for hydraulic models and can be improved with various remote sensing technologies, such as the use of high-resolution imagery and several data sources from other satellite imagery. This method enhances the accuracy of flood risk assessment due to the effects of land subsidence by using a high-resolution Digital Terrain Model (DTM) to obtain watershed morphometric parameters needed for flood distribution mapping[22,23]. One of the important parameters needed in the calculation of hydrological analysis and flood tracking is the determination of the concentration time required for a water flow from the source to the watershed outlet.

In this context, Sentinel 1 remote sensing imagery offers information for the accurate determination of land subsidence, land use, and fast data collection, essential in flood-prone areas. HEC-RAS (Hydrologic Engineering Center's River Analysis System) is also used due to the ability to perform 1D and 2D hydraulic calculation analysis, as well as integration with high-resolution DTM data to improve the accuracy of elevation change parameters and flood risk estimates [24]. Additionally, Sentinel 1 remote sensing imagery is effective for measuring and quantifying land subsidence [25,26]. This is particularly relevant for Lambidaro downstream sub-watershed in Palembang City where land subsidence has been significant. Over the past decades (2019-2024), the Lambidaro sub-watershed has experienced a cumulative height change of -40,1 to - 50 cm in the watershed area [27], characterized by an insignificant riverbed channel.

2. RESEARCH SIGNIFICANCE

Lambidaro river subsystem is among the 21 river subsystems that form flow patterns in Palembang city [28]. In addition to the low topography of (1.0 m to 14.5 m) msl, this area has the potential for significant land subsidence, around -30 – 40 cm in the period 2023-2024 [29]. In 2018, the number of flood locations increased with a depth of 20 to 50 cm and a duration of ± 10 hours. This shows the need to address the problem of flooding and inundation by considering changes in land use, drainage ability, the condition of soil, precipitation, the intensity of rainfall, and adaptation to land subsidence.

3. DATA AND METHOD

3.1 Land Use

The left Lambidaro river subsystem, with an area of 29,489 Km2, has different morphometric characteristics from the others. Based on the flow pattern, it is divided into two river subsystems, namely the left and right Lambidaro, which meet in the downstream area and flow into the Musi River. The morphometric characteristics of the left Lambidaro river subsystem are shown in Fig. 1 and Table. 1, with land use dominated by shrubs, trees, fields, and forests accounting for 78.80%. Meanwhile, swamps, ponds, lakes, and rivers are 21.20%, showing potential for infrastructure and settlement development.

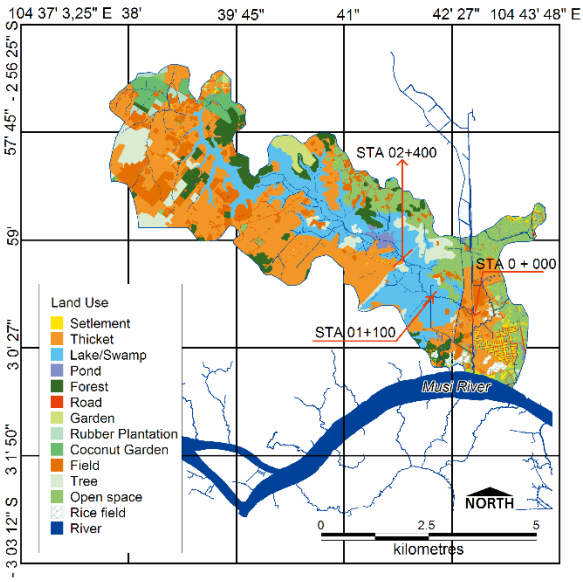

Fig. 1 Land use map and infiltration coefficient values of the left Lambidaro river sub-system area

Until the end of 2024, the occupation of swamp land for the central government area, education, and settlements will become wider by filling in swamps. Settlement development mainly occurs along the main road/outer ring road of Palembang City (Musi 2 to Jambi). The Lambidaro river sub-system has a varying height of less than 2.5 m and 14 m above mean sea level (MSL) in the downstream and upstream estuary areas, respectively. The slope gradient is dominated by less than 3%, and the condition of the river is still natural. However, some rivers in the upstream part of the watershed have been normalized by strengthening the banks.

Table 1. Calculation of CN value and infiltration percentage

Land Use	Km2	CN	AxCN	%	Ci
River	0,160	72	11,523	2	0,011
Rubber Plantation	0,222	79	17,569	5	0,038
Rice field	0,347	88	30,563	2	0,024
Pond	0,365	72	26,252	2	0,025
Road	0,380	90	34,176	100	1,288
Garden	0,476	88	41,929	5	0,081
Settlement	0,533	95	50,662	85	1,537
Coconut Plantation	0,872	79	68,882	5	0,148
Tree	1,769	79	139,737	5	0,300
Forest	1,961	76	149,004	5	0,332
Field	2,774	88	244,073	2	0,188
Open Space	4,000	80	320,018	2	0,271
Lake/swamp	5,726	72	412,308	2	0,388
Thicket	9,904	77	762,579	5	1,679
Sum	29,489		2.309,274		6,310

Based on Table 1, the average CN (Composite Number) value and the percentage of the average impermeable area at the location can be calculated.

The average CN value for the area of the rain catchment area is:

$$C_{CA} = \frac{\sum_{i=1}^{n} C_i A_i}{\sum_{i=1}^{n} A_1} = \frac{2309.274}{29.489} = 78{,}309$$

CN was calculated using the conditions of land use, slope gradient, flow density, soil type, and the range of runoff coefficient values in the left Lambidaro river subsystem, as shown in Fig. 2 the combined CN value obtained is 78.309 from the graph of the relationship between the impervious area (27.67%) and the composite CN (80).

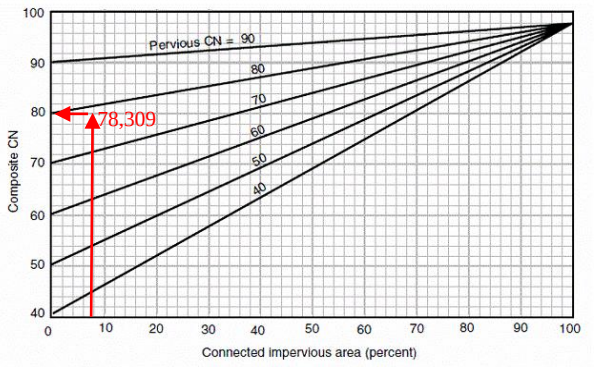

Fig. 2 Graph of the relationship between impervious area and CN

3.2 Effective Rain

The Hyetograph ABM rainfall data with a return period of 25 years were used to calculate effective rainfall (*Pe*) using the SCS-CN method. The cumulative (*P*) calculation of losses and effective rainfall are shown in Fig 3.

3.3 Method

Sentinel 1 Satellite data processing, using the D-InSAR method was applied to obtain land subsidence for the period 2014-2024. Land Subsidence was obtained through the integration of high-resolution Large Format Aerial Photographs (0.25 m) and satellite-based GNSS measurements.

This was carried out by combining cumulative land subsidence data obtained through the D-InSAR method during 2014–2024.

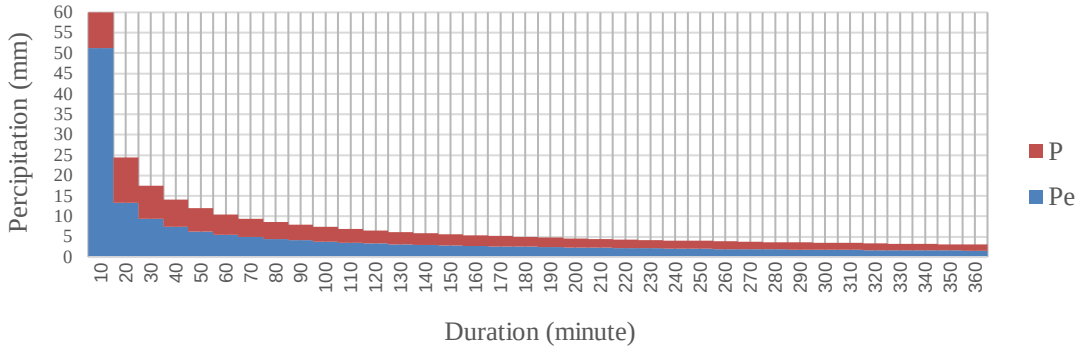

Fig. 3 Graph of the relationship between effective rain (*Pe*) and ABM Hyetograph rain (*P*)

The results of the hydraulic model were used to assess flood changes by considering the impact of land subsidence. Fig. 4 shows a flow diagram of the research methodology used and other data as input for modeling. Section 2 provides an explanation for the model.

Section 3 explains the influence of floods to categorize risks based on depth.

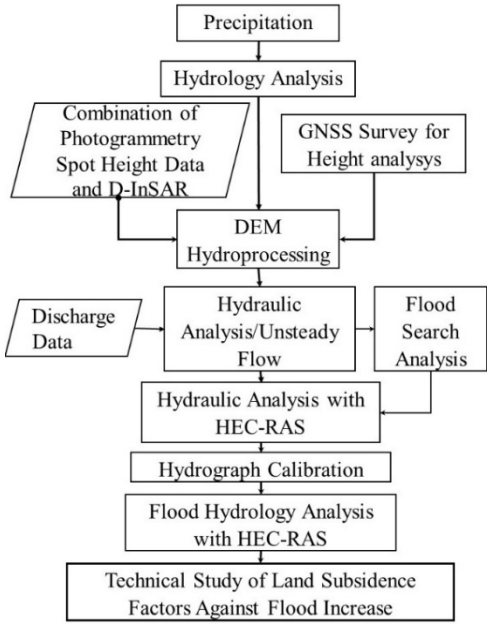

Fig. 4 Research flow diagram

4. RESULTS AND DISCUSSION

4.1. D-InSAR Data Analysis

In this research, land subsidence data processed from Sentinel 1 Satellite imagery using the D-InSAR method were combined with data from the interpretation of Small Format Aerial Photos to achieve a cumulative dataset based on temporal deformation from 2014 to 2024. As shown in Fig. 5, six transverse profile lines intersected the Long Section 1 profile line, from the BM UNSRI-P10 monitoring point towards BM-UNSRI-P11, in the Lambidaro sub-watershed. The area traversed by these profile lines experienced significant subsidence towards the center of the map, showing the center of Palembang City. The maximum subsidence value of -50 cm occurred in Palembang City along the Cross section 6 profile line, which was 4.68 km. Meanwhile, the minimum subsidence of -6 cm intersected by Cross section 5 and 6 profile lines, spanning 4.80 km and 5.03 km, respectively.

Based on Table 2, the maximum subsidence of -51.6 cm occurred between April 2022 to 2024, as shown Fig. 6 by a color that tends to range from apple green to dark purple. The minimum subsidence of -40.1 cm occurred from 2022 to 2024.

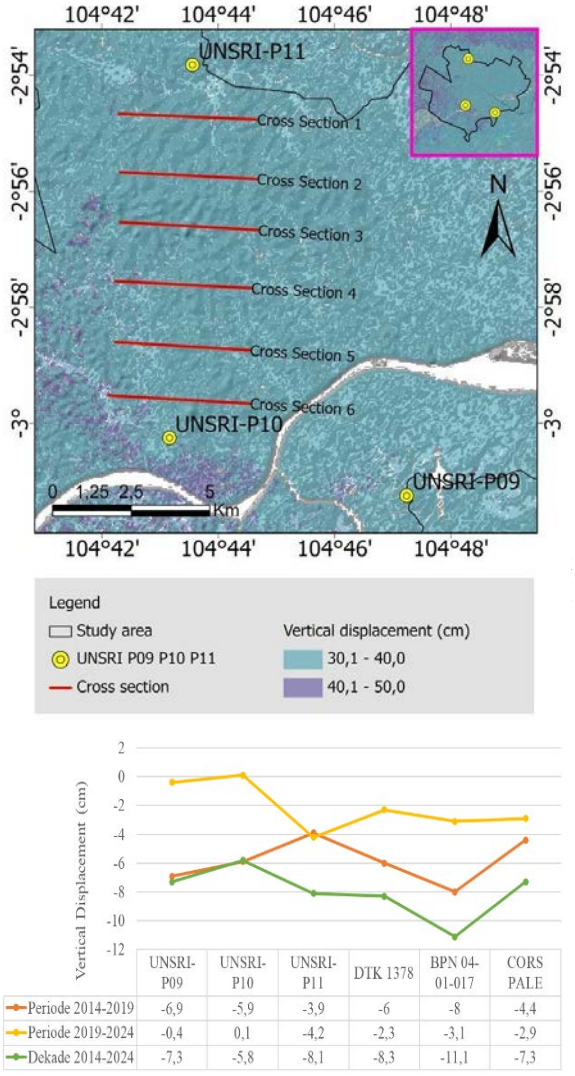

Fig. 5 Cross section 5 and 6 is the displacement at Lambidaro river sub-system during August 2014-2024.

Table 2. Vertical displacement value of Palembang City for the period 2014 to 2024.

Period	Vertical Displacement Palembang City (Cm)				Vertical Displacement Palembang City and surrounding areas (cm)
	Subsidence		Uplift		
	Min	Max	Min	Max	
2014-2016	0	-14.1	0	+04.0	-14.1 – 10.0
2016-2018	0	-11.4	0	+09.0	-11.4 – 26.1
2018-2020	0	-14.7	0	+03.0	-14.7 – 3.0
2020-2022	0	-13.1	0	+10.0	-13.1 – 10.0
2022-2024	0	-40.1	0	+06.0	-40.1 – 51.6

Additionally, the research area experienced an uplift or maximum topographic increase in the period

of September 2022 to November 2024, amounting to +06.0 cm, as shown by a purplish blue color. This can be caused by several swamp fillings and the elevation of the Palembang-Jambi Outer Ring Road which passes through the left Lambidaro river sub-systems using reeget pavement.

4.2. Synthetic Unit Hydrograph With SCS Method

This research used dimensionless synthetic unit hydrograph (HSS) such as Soil Conservation Service (SCS), where the discharge is expressed as discharge (q) against peak discharge (Qp) and time (t) against the rise time of the unit hydrograph (Tp). When the Qp and the delay time for an effective rainfall duration are known, the unit hydrograph can be estimated. During the experiment, a rainfall-runoff simulation was carried out in the Lambidaro sub-system area. The ABM Hyetograph rainfall data with a return period of 25 years were applied to calculate effective rainfall using the SCS-CN method. Discharge was expressed as (q) against (Qp) and (t) against the rise time of the unit hydrograph (Tp). When the Qp and the delay time for an effective rainfall duration are known, the unit hydrograph can be calculated.

The parameters used in calculating the HSS-SCS of the left Lambidaro sub-watershed are as follows:

River length (L) = 6.54 km
Maximum potential retention (S) = 2,048 inch
Average slope (Y) = 0.05%
Watershed area (A) = 29.49 km^2

a. *Time Lag* (t_L) or break time

$$t_L = \frac{L^{0,8}\times(S+1)^{0,7}}{1900\,.\,Y^{0,5}}$$

$$= \frac{\mathbf{26540^{0,8}}\times(\mathbf{2,048+1})^{\mathbf{0,7}}}{\mathbf{1900\,.\,0,05^{0,5}}}$$

= 4,387 hour

b. *Time to Concentration* (t_c)

$$t_c = \frac{L^{0,8}\times(S+1)^{0,7}}{1140\,.\,Y^{0,5}}$$

$$= \frac{6540^{0,8}\times(2,048+1)^{0,7}}{1140\,.\,0,05^{0,5}}$$

= 7,312 hour

c. Duration of rain (t_r)

t_r = 0,133 . t_c
= 0,133 . 7,312
= 0,973 hour

d. Time to Peak (t_p)

t_p = t_L + 0,5 t_r
= 4,387 + 0,5 . 0,081
= 4,873

e. Peak discharge (Q_p)

$$Q_p = \frac{\mathbf{0,208\times A}}{\mathbf{t_p}}$$

$$Q_p = \frac{\mathbf{0,208\times 29,49}}{\mathbf{4,873}} = 1,2587\ m^3/s$$

Based on the calculation using the SCS method, the peak discharge is 1.2587 m^3/second for every 1 mm of rainfall. The HSS SCS graph is shown in Fig. 6.

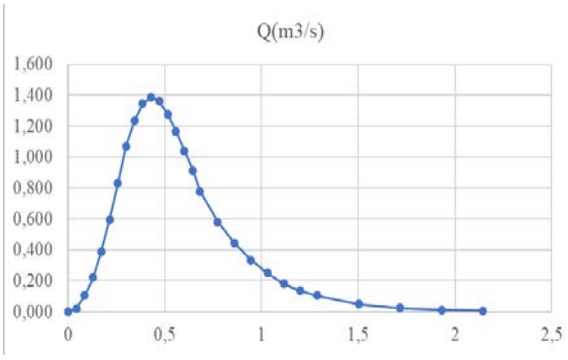

Fig 6. SCS synthetic unit hydrograph

4.3. Direct Runoff Discharge Calculation in The Left Lambidaro River Subsystem

The calculation of direct runoff discharge is designed using a 25-year return period with a 10-minute interval for eight hours. Based on the results of the direct runoff hydrograph, a peak discharge of 47.472 m^3/s was obtained within 30 th minute.

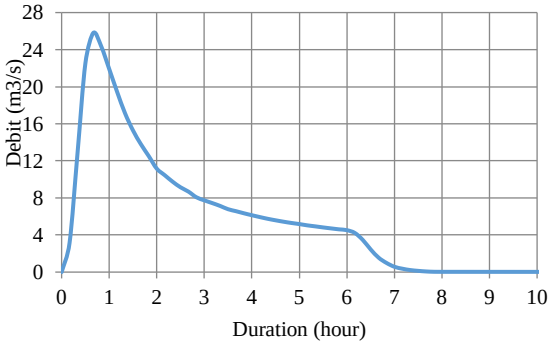

Fig 7. Direct run-off hydrograph of left Lambidaro river sub system

4.4. Modeling With HEC-RAS

In the modeling of the Lambidaro river, the left is divided into the upstream and downstream parts. In

addition to the flow scheme, there are also retention ponds as shown in Fig. 8.

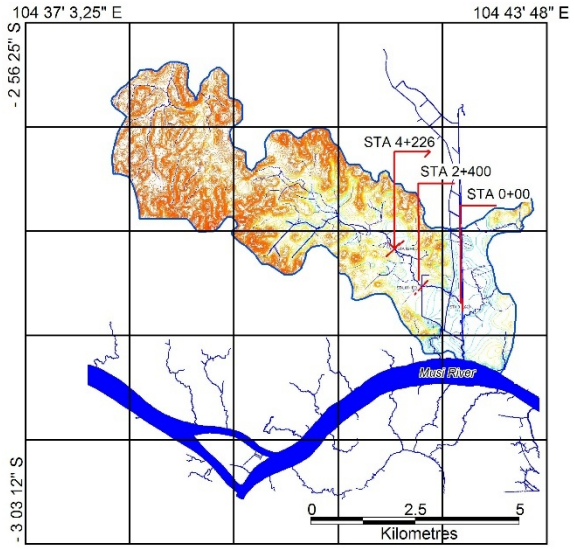

Fig 8. New elevation and Schematic of the Lambidaro river sub system flow

Table 3. STA channel in HEC-RAS modeling

STA Channel Name	STA	
	start	End
Lower Lambidaro	0+000	1+100
Midle Lambidaro	1+100	2+400
Upper Lambidaro	2+400	4+226

The results of the 2D flood simulation in the Lambidaro river sub system using run-off hydrograph data for the cross section of the lower and midle Lambidaro river sub system channel STA 0+00 to STA 2+400 are shown in Fig. 9.

Table 4. Water level profile calculation of lower and middle left Lambidaro river sub system channel

No.	STA	Flood Level Elevation (m)	River Bank height (m)	Flood Height (m)
1	0+000	3	1	2
2	0+100	3	1	2
3	0+200	3	1	2
4	0+300	3	1,5	1,5
5	0+400	3	2	1
6	0+500	2	2,5	0,5
7	0+600	2	2,5	0,5
8	0+700	1,5	1	0,5
9	0+800	1,5	1	0,5
10	0+900	1,5	0,5	0,5
11	1+000	1,5	0,5	1
12	1+100	1,5	0,5	1
13	1+200	1,5	0,5	1
14	2+000	1,5	0,5	1
15	2+400	1,5	0,5	1

The HEC-RAS model simulation was conducted on the Lambidaro river subsystem.

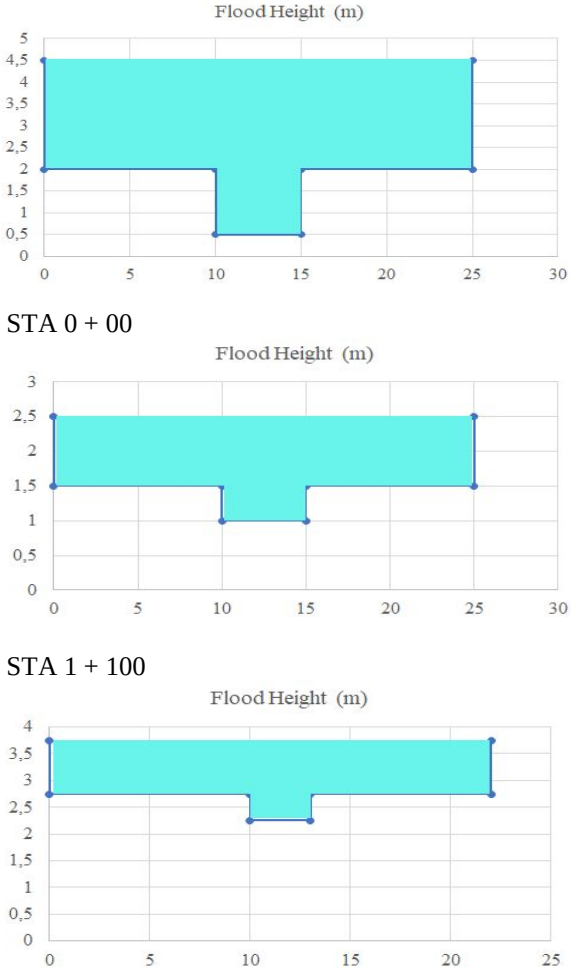

Fig.9 Cross section of the inundation height search using the HEC-RAS method

Schematic of the water system network was based on DEM extraction with flow patterns producing river subsystem boundaries and drainage lines to describe flood runoff (Fig. 10).

The results of inundation distribution analysis in the Lambidaro river subsystem are grouped into six classifications. These include (1) areas that are not inundated, as well as (2) inundated with a height of less than 0.25 m, (3) 0.25 - 0.5 m, (4) 0.5-0.75 m, (5) 0.75-1 m, and (6) a height of more than 1 m. The results of the hydrodynamic modeling using the HEC-RAS model which is continued with an analysis of the distribution of inundation that will occur with a 25-year return period scenario are shown in Fig. 10.

Fig. 10 shows the spatial distribution of water depth differences. Based on the results, the largest differences are concentrated in the downstream area due to its proximity with the highest cumulative land subsidence, which shows water depth ranging from 1–2 m and velocity greater than 0.35 m/s.

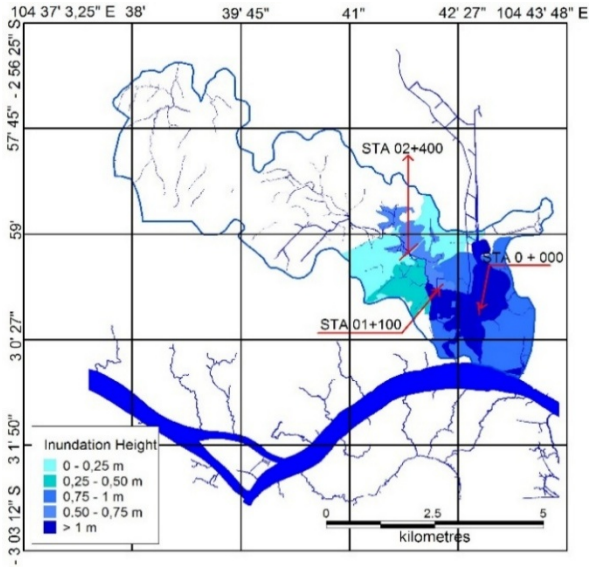

Fig 10. Distribution of inundation in the downstream left Lambidaro river subsystem

The maximum difference in water depth to approximately 2 m corresponds to the variation of 2.5 m between the two analyzed scenarios. The most affected zones are mostly occupied by settlements, farming, and fisheries activities in the downstream area. Furthermore, residential areas along the Bukit Sejahtera outer ring road, as well as the surroundings, show extensive changes in inundation, predominantly occurring near the river in the lowlands with land subsidence.

5. CONCLUSION

In conclusion, this research showed that the boundary of the river subsystem flow pattern was the basis for analyzing the condition of the river subsystem structure. The results obtained were as follows.

1. Based on DTM data and a pixel size of 5m x 5m, the morphometry of the river subsystem was obtained according to the actual flow pattern conditions in the field.
2. The spatial relationship between changing land use, river morphometry, and the influence of surface water runoff and river tides was expressed in the form of inundation distribution (area and height of inundation) with a return period of 25 years.
3. The control pattern of the Lambidaro river subsystem, with over 70% green space and swamps, was still very possible with a non-structural method such as land use regulation, the construction of a new and larger retention pond.

6. ACKNOWLEDGMENTS

The authors are grateful to the Directorate of Research Technology and Community Service, Directorate General of Higher Education, Research and Technology, Ministry of Education, Culture, Research and Technology, the Republic of Indonesia, who has provided research funding through Doctoral Research grants based on Master Contract No.:090/E5/PG.02.00.PL/2024, Date : June 11, 2024 and Derivative contract No. 0016.006/UN9/SB1.LP2M.PT/2024, Date June 19, 2024.

7. REFERENCES

[1] Bott L.M, Schöne. T, Illigner. J, Haghshenas Haghighi. M, Gisevius. K, and Braun, B, Land Subsidence in Jakarta and Semarang Bay – The relationship between physical processes, risk perception, and household adaptation, Ocean Coast. Manag., Vol. 211, 2021, doi: 10.1016/j.ocecoaman.2021.105775.

[2] Bagheri. M, G, Hosseini S.M, Ashtiani B.A, Sohani. Y, Ebrahimian. H, Morovat. E, Ashrafi S. Land subsidence : A global challenge, Sci. Total Environ., vol. 778, 2021, doi: 10.1016/j.scitotenv.2021.146193.

[3] Rapalo. L.M.C, Uliana. E.M, Moreira. M.C, Silva. D.D, Melo.C.B, Cruz. I.F, Pereira. D.D.R.P, Effects of land-use and cover changes on streamflow regime in the Brazilian Savannah, Journal of Hydrology. Regional. Study., vol. 38, October, p. 100934, 2021, doi: 10.1016/j.ejrh.2021.100934.

[4] Tomás L, Fonseca. L, Almeida. C.M, Leonardi. F, and Pereira. M, Urban population estimation based on residential buildings volume using IKONOS-2 images and lidar data, International Journal of Remote Sensing., vol. 37, no. 1, pp. 1–28, 2016, doi: 10.1080/01431161.2015.1121301.

[5] Yulaikhah. S, Pramumijoyo, Widjajanti. N, and Widagdo. A, Optimal design of the Sermo Fault deformation monitoring network using sensitivity criteria based on geological information, Arab. J. Geosci., vol. 14, no. 20, 2021, doi: 10.1007/s12517-021-08411-6.

[6] Deros S.N.M, Din, N.M, Norzeli. S.M, Omar. R.C, Usman. F, and Hamim. S.A, Land Subsidence Susceptibility Projection for Palembang Slum Area by Complex MCDM-AHP Technique, Journal Engineering Technology. Sci., vol. 54, no. 1, 2022, doi: 10.5614/j.eng.technol.sci.2022.54.1.4.

[7] Putranto. D.D.A, Sarino, Yuono. A.L, Juliana. I.C, and Hamim. S.A, Integration of surface water management in urban and regional spatial planning, International. Journal of GEOMATE, vol. 14, no. 45, pp. 28–34, 2018, doi: 10.21660/2018.45.18652.

[8] Feng S, Zhao. W, Zhan. T, Yan.Y, and Pereira. P, Land degradation neutrality: A review of progress and perspectives, Ecol. Indic., vol. 144, no.4, September, p. 109530, 2022, doi: 10.1016/j.ecolind.2022.109530.

[9] Giuliani G, Chatenoux. B, Benvenuti. A, Lacroix. P, Santoro. M, and Mazzetti. P, Monitoring land degradation at national level using satellite Earth Observation time-series data to support SDG15 –

exploring the potential of data cube, Big Earth Data, vol. 4, no. 1, pp. 3–22, 2020, doi: 10.1080/20964471.2020.1711633.

[10] Cian F, Blasco. J.M.D, and Carrera. L, Sentinel-1 for monitoring land subsidence of coastal cities in Africa using PSInSAR: A methodology based on the integration of SNAP and staMPS, Geosci., vol. 9, no. 3, pp. 1–32, 2019, doi: 10.3390/geosciences9030124.

[11] Andriani, Ibrahim. E, Putranto. D.D.A, and Affandi. A.K, Evaluation of Land Subsidence Impact at Lowland Areas Using Analitycal Hierarchy Process (AHP) Method, E3S Web Conf., vol. 68, pp. 1–7, 2018, doi: 10.1051/e3sconf/20186804017.

[12] Putranto D.D.A, Fitriani H, and Andriani, Analysis of carrying capacity of land for special economic zones tanjung api-api in infrastructure development," Int. J. Sci. Technol. Res., vol. 9, no. 2, pp. 1248–1253, 2020.

[13] Muchtar. Z, Putranto D.D.A, Hadinata F, and Bastian L, The Effect of Changes in Land Use on The Prediction of Critical Land Distribution in The Rawas Watershed (South Sumatra Province , Indonesia, 12th Int. Conf. on GEOMATE 2022, November, pp. 22–24.

[14] Yustiana. F, Ridwanullah M.H, Kurniadi, Y.N, Wardhani E, Widyaningsih E, and Author C, HEC-RAS Model For Drainage Capacity Analysis and Peak Discharge Simulation of Cimande River, vol. 27, no. 123, pp. 30–37, 2024.

[15] Febrita Y, Ekasiwi S.N, and Antaryama I.G.N, Impact of Urban River Dynamics on Microclimate: Climatic Factors Along the Martapura River, International. Journal of GEOMATE, vol. 27, no. 121, pp. 56–68, 2024, doi: 10.21660/2024.121.4508.

[16] Hutanu. E, Mihu-Pintilie. A, Urzica A, Paveluc L.E, Stoleriu C.C, and Grozavu A, Using 1D HEC-RAS modeling and LiDAR data to improve flood hazard maps accuracy: A case study from Jijia Floodplain (NE Romania), Water (Switzerland), vol. 12, no. 6, pp. 1–21, 2020, doi: 10.3390/w12061624.

[17] Suif. Z, Jelani. J and Ahmad, N, GIS and Remote Sensing Integration for Soil Erosion Assessment Based on a Rusle Model in Upnm Catchment, Int. J. GEOMATE, vol. 26, no. 114, pp. 84–91, 2024, doi: 10.21660/2024.114.G13380.

[18] Sahdar. I, Rohmat. D, Pranoto W.A, and Solehudin, Hydraulic Modeling for Flood Control Scenarios in Akelaka Watershed, North Maluku, Indonesia, Int. J. GEOMATE, vol. 27, no. 120, pp. 49–59, 2024, doi: 10.21660/2024.120.4450.

[19] Mengye Chen, Zhi Li, Shang Gao, Ming Xue, Jonathan J.G, Randall , Kolar, Yang Hong, A flood predictability study for Hurricane Harvey with the CREST-iMAP model using high-resolution quantitative precipitation forecasts and U-Net deep learning precipitation nowcasts, Journal. Hydrol., vol. 612, no. PB, p. 128168, 2022, doi: 10.1016/j.jhydrol.2022.128168.

[20] Sarchani. S, Seiradakis. K, Coulibaly. P, and Tsanis. I, Flood Inundation Mapping in an Ungauged Basin, Water, vol. 12, no. 6. 2020, doi: 10.3390/w12061532.

[21] Jiang H, Zhang. J, Liu. Y, Li. J, and Fang. Z.N, Does flooding get worse with subsiding land ? Investigating the impacts of land subsidence on flood inundation from Hurricane Harvey, Sci. Total Environ., vol. 865, 2023, doi: 10.1016/j.scitotenv.2022.161072.

[22] Julzarika, Aditya. C.A, Subaryono, and Harintaka, Dynamics Topography Monitoring in Peatland Using the Latest Digital Terrain Model, J. Appl. Eng. Sci., vol. 20, no. 1, pp. 246–253, 2022, doi: 10.5937/jaes0-31522.

[23] García-Alén G, González-Cao. J, Fernández. D.N, Gómez-Gesteira. M, Cea. I, and Puertas. J, Analysis of two sources of variability of basin outflow hydrographs computed with the 2D shallow water model Iber: Digital Terrain Model and unstructured mesh size, J. Hydrol., vol. 612, no. April, 2022, doi: 10.1016/j.jhydrol.2022.128182.

[24] Venkatcharyulu. S and Viswanadh. G.K, Runoff volume model for Godavari sub-basin using HEC-RAS software, Model. Earth Syst. Environ., 2021, doi: 10.1007/s40808-021-01311-4.

[25] Kamali E. Papoutsis. I.M, Loupasakis,. C, Abuelgasim. A, Omari. K, and Kontoes. C, Monitoring of land surface subsidence using persistent scatterer interferometry techniques and ground truth data in arid and semi-arid regions, the case of Remah, UAE, Sci. Total Environ., vol. 776,p.145946,2021, doi: 10.1016/j.scitotenv.2021.145946.

[26] Xiong. J, Xiao R, and He. X, Land surface deformation in Nanchang, China 2018–2020 revealed by multi-temporal InSAR, Nat. Hazards Res., vol. 1, no. 4, pp. 187–195, 2021, doi: 10.1016/j.nhres.2021.10.003.

[27] Artini. S.R, Rosidawani, Putranto. D.D.A, Integrating Geodetic Control Points and Spatiotemporal Variation in Monitoring Land Subsidence in Sub-Optimal Terrain., 13th Int. Conf. on Geotechnique, Construction Materials & Environment, Tsu Mie, Japan, November,2023. pp. 947-952.

[28] Firdaus, Putranto. D.D.A, and Juliana I.C, A combined hydrological and hydraulic model for flood prediction in Buah river subsystem area, Palembang city, Int. J. Adv. Technol. Eng. Explor., vol. 9, no. 88, pp. 270–285, 2022, doi: 10.19101/IJATEE.2021.875067.

[29] Artini S.R, Rosidawani, Putranto. D.D.A, City Development and Land Success Problems in River Delta Areas, International Journal of Religions, vol. 5, no. 12, 2024. pp. 364-375. doi: https://doi.org/1061707/q15atn92.